Flame Boundary Measurement Using an Electrostatic Sensor Array

Authors: Jiali Wu [a]

Yong Yan [b] (Corresponding author)

Yonghui Hu [a]

Shan Li [a]

Weicheng Xu [a]

Addresses: [a] School of Control and Computer Engineering

North China Electric Power University, Beijing 102206, China

[b] School of Engineering and Digital Arts

University of Kent, Canterbury, Kent CT2 7NT, U.K.

Tel: 00441227823015

Fax: 00441227456084

Email: y.yan@kent.ac.uk

ABSTRACT

Flame boundary is an important geometrical characteristic for the evaluation of flame properties such as heat release rate and radiation. Reliable and accurate measurement of flame boundary is desirable for the prediction of flame structure and the optimization of combustion systems. Such measurement will inform the designers and operators of the combustion systems. This paper presents for the first time a study of using an electrostatic sensor array for flame boundary measurement. The electrostatic sensor is placed in the vicinity of the flame to sense its movement through charge transfer. The principle, design, implementation and assessment of a measurement system based on this methodology are introduced. Comparative experimental investigations with a digital camera conducted on a laboratory-scale combustion test rig show that the electrostatic sensor can respond to the variation of the distance between the electrode and the flame boundary. Reconstruction of the flame boundary is achieved using a set of distance measurements obtained from a sensor array. For diffusion flames over the range of fuel flow rate 0.60-0.80 L/min and premixed flames over the range of equivalence ratio 1.27-3.81, experimental results show that the measurement system is capable of providing reliable measurement of the flame boundary. The correlation coefficients under all test conditions are mostly larger than 0.96, the mean relative errors within 7.4% and the relative root mean square errors within 0.09. More accurate flame boundary measurements are achieved for diffusion flames. In addition, the overall polarity of charges in a flame can be determined from the polarity of the sensor signal.

Index Terms– Flame boundary; electrostatic sensor; sensor array; boundary measurement; combustion monitoring.

I. INTRODUCTION

A flame is the central reaction zone of a combustion process. The geometrical characteristics of a flame are essential for the determination of its structural properties and the estimation of its thermal impact (i.e., convection and radiation) to the surroundings [1]. There has been a long history of characterizing the geometrical features of a burner flame in combustion research [1-4], such as flame shape, boundary, length, width, tilt, surface area, structure, location and front thickness, etc. Among these characteristics, flame boundary is an important indicator of flame properties such as heat release rate and radiation [2]. In addition, the flame boundary forms a basis of the quantitative determination of such flame geometrical parameters. Therefore, reliable and accurate measurement of flame boundary is desirable for the prediction of flame structure, the fundamental understanding of reaction processes and the optimization of combustion systems.

Over the last few decades, a variety of methods have been developed for the measurement of flame boundary, such as laser-based imaging, chemiluminescence imaging and direct photographic techniques. Planar laser induced fluorescence (PLIF) from the OH radicals in the flame was used to determine the boundary of the turbulent premixed conical flames [5]. Parsinejad *et al*. captured the shadowgraph and schlieren images of the flame to detect the exact location of the boundary in expanding spherical flames [6, 7]. However, the laser-based techniques require seeding or extra lighting source, which are impractical for routine industrial applications. Chemiluminescence imaging techniques, which avoid the need for external illumination or seeding, capture radiative emission from electronically excited species formed by thermal excitation and chemical reactions in the flame to measure flame boundary. Hardalupas *et al.* used photography and chemiluminescence from CH radicals to quantify the flame boundary and identify the reaction zones [8]. The direct photographic techniques using CCD (charge-coupled device) cameras capture

the radiation naturally emitted by a flame and have been recognized as feasible approaches for flame boundary measurement in practical furnaces [9]. Several methods have been proposed to extract the flame boundary from flame images, such as Roberts, Prewitt, Sobel, Log and Canny operators [10, 11]. These optical techniques capturing flame images can provide rich information, such as flame geometric, luminous and thermodynamic parameters. However, such techniques are primarily based on the optical properties of flames and seldom rely on their electrical properties.

It is well known that a large amount of charged species is created when hydrocarbon fuels burn. These charged species will modify the permittivity and conductivity of the combustion volume [12]. Preliminary research on electrical properties of a burner flame [13-15] has been conducted to determine its characteristics, including ion density and distribution, flame location and oscillation frequency. A negatively biased conducting plate or sensing probe that uses the burner as a reference electrode has been used to measure the ion density and its distribution in a flame [13]. Ion-current sensors have been adopted for the measurement of the oscillation frequency of a burner flame [14]. By exploiting these charged species, Waterfall *et al.* developed an electrical capacitance tomography system to reconstruct the cross-section of the flame in a scaled model of an internal combustion engine. [15]. However, all such sensors apply an external electric field to the flame, which can adversely affect its stability, shape and burning rate.

The electrostatic sensor offers a good potential for the characterization of electrical properties of burner flames owing to its advantages of passive detection, structural simplicity, cost-effectiveness, and suitability for applications in hostile environments. To date, there has been no reported research in the literature on flame boundary measurement using electrostatic sensors. Electrostatic sensors have been extensively used for the measurement and characterization of particle flow in pneumatic conveying pipelines and fluidized beds [16-17]. Recent studies have been reported on the

applications of electrostatic sensors to rotational speed [18], belt speed and vibration measurement [19]. In this paper, an electrostatic sensor array is adopted for the first time to achieve flame boundary measurement. The sensor array is placed in the vicinity of the flame to sense its movement. The flame boundary is reconstructed from a set of measurements of the distance between the electrode and the flame boundary. This paper presents the fundamental principle, design and implementation of the system. Meanwhile, the measurement system is assessed on a gas fired test rig for diffusion and premixed flames.

II. Measurement Principle and Sensor Design

A. Electrical Property of a Flame

Burner flames are highly conductive because of the existence of positive and negative ions, electrons as well as charged soot particles [12]. It is well known that electrons and ions are created in a flame via chemi-ionization reactions, which are sufficiently exothermic to ionize the reaction products [20]. The dominant chemi-ionization reaction in a hydrocarbon flame can be described as [20, 21],

$$CH+O \rightarrow CHO^{+}+e^{-} \quad (1)$$

The CHO^{+} then quickly reacts further to produce H_3O^{+}, $C_3H_3^{+}$and other secondary hydrocarbon ions [21],

$$CHO^{+}+H_2O \rightarrow H_3O^{+}+CO \quad (2)$$

$$H_3O^{+}+C_3H_2 \rightarrow C_3H_3^{+}+H_2O \quad (3)$$

A significant fraction of soot particles formed in a flame are also charged [22]. The chemiion, $C_3H_3^{+}$, rapidly grows by the addition of acetylene or other neutral species to form increasingly larger ions which either become incipient charged soot particles or combine with electrons (produced in the

chemi-ionization process) to produce incipient neutral soot particles. These particles, neutral or charged, continue to grow by the addition of acetylene. In a hot flame, the particles become charged due to thermal ionization or diffusive charging. Some electrons produced in Reaction (1) produce negative ions by attaching to large molecules [23].

Although the flame is a weak plasma and electroneutral as a whole [24], the density and species of ions, electrons and charged soot particles vary in different regions of a flame. Moreover, the spatial distribution of ions, electrons and charged soot particles varies with time due to the instability of the combustion process and the complex interaction between gaseous and solid phases. Therefore, information about the combustion process can be obtained by sensing the ions, electrons and charged soot particles in the flame.

B. Measurement Principle

Fig. 1 illustrate the sensing arrangement and principle of the flame boundary measurement system developed in this study. An array of electrostatic sensors is placed in the proximity of the flame. The ions, electrons and charged soot particles generated in the flame contact with the exposed electrode, and then charges are transferred to the surface of the electrode. Due to the motion of such charged species in the flame, induced charge is also generated on the electrode through electrostatic induction. The amount of transferred and induced charges on the electrode depends on a variety of factors, such as the concentration of ions, electrons and charged soot particles generated in a hydrocarbon flame and the change of the flame shape. For fixed operation conditions, the variation of charge concentration in a flame is very small. If the flame shape remains unchanged, the spatial charge density around the electrode can be regarded as constant. However, the flame shape changes constantly with time, resulting in the variation of the distance between the electrode and the flame boundary and hence the variation of the spatial charge density around the electrode. It is therefore

deduced that the fluctuation of the electrostatic signal is mainly influenced by the variation in the distance between the electrode and the flame boundary. As a result, the closer the distance between the electrode and the flame boundary, the more transferred charges on the electrode and the stronger the output signal. The information about the variation of the distance between the electrode and the flame boundary can thus be derived.

In order to acquire the absolute distance between the electrode and the flame boundary, the relationship between the sensor signal and the distance should be determined in advance. Due to the complex mechanism of charge generation and distribution, the relationship cannot be established analytically. Calibration of the measurement system is therefore required in order to derive the absolute distance under different operating and environmental conditions. In this study, regression analysis is performed to determine the relationship between the sensor signal and the distance. The reference distance measured using a digital CMOS camera and the average magnitude of the sensor signal are regressively analyzed to obtain the regression equation. Due to the localized sensing zone, the electrostatic sensor measures distance at only a single point. In order to measure the flame boundary, multiple electrostatic sensors arranged in a linear array along the flame longitudinal direction are employed. The electrostatic sensors are labelled as S_i (i = 1, 2, …, n), where n is the number of the electrostatic sensor which is determined by considering the size of the flame and the requirement for measurement accuracy. When a set of distance measurements from the electrostatic array are obtained, the flame boundary is reconstructed.

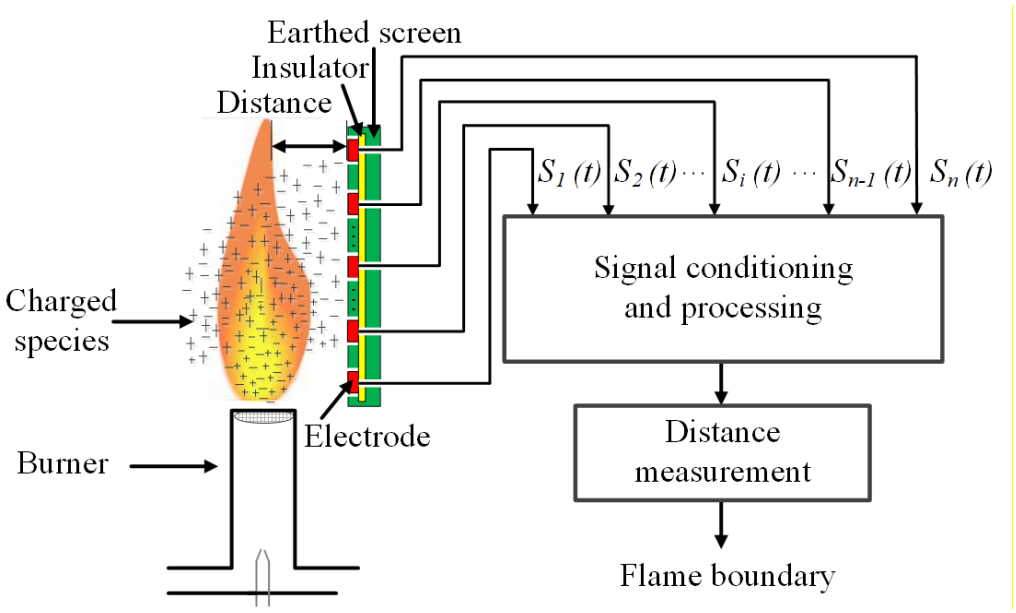

Fig. 1. Sensing arrangement and principle of the flame boundary measurement system.

C. Sensor Design and Signal Conditioning

Fig. 2 shows the design and construction of the electrostatic sensing system. It consists of an electrostatic sensing head, a signal conditioning unit and an earthed metal screen. The entire system was constructed in-house by the authors. A total of 20 strip-shaped, exposed electrodes and a quartz insulating plate are housed in the metal sensing head. The metal electrodes have the same dimensions of 20 mm in length and 3 mm in width. The length of the electrode is slightly wider than the diameter of the measured flame, and its width determines the spatial resolution along the flame axis. The center-to-center spacing between two adjacent electrodes in parallel is 10 mm. The earthed screen is designed to support the electrode and minimise external electromagnetic interference. The electrodes are numbered as S_1, S_2, …, and S_{20}, in the direction from the flame root to the flame tip, respectively. Since the temperature around the flame is at least several hundred degrees Celsius, which is beyond the thermal tolerance of a common printed circuit board, the sensing head is thus thermally isolated from the circuit board, as shown in Fig.2. The thermal

isolation is achieved through a hollow structure of the sensing head (Fig.2(b)) with a depth of 50 mm and a copper tube connection with a length of 100 mm between the sensing head and the signal conditioning unit (Fig.2(c)). The copper tube also serves to eliminate external electromagnetic interference.

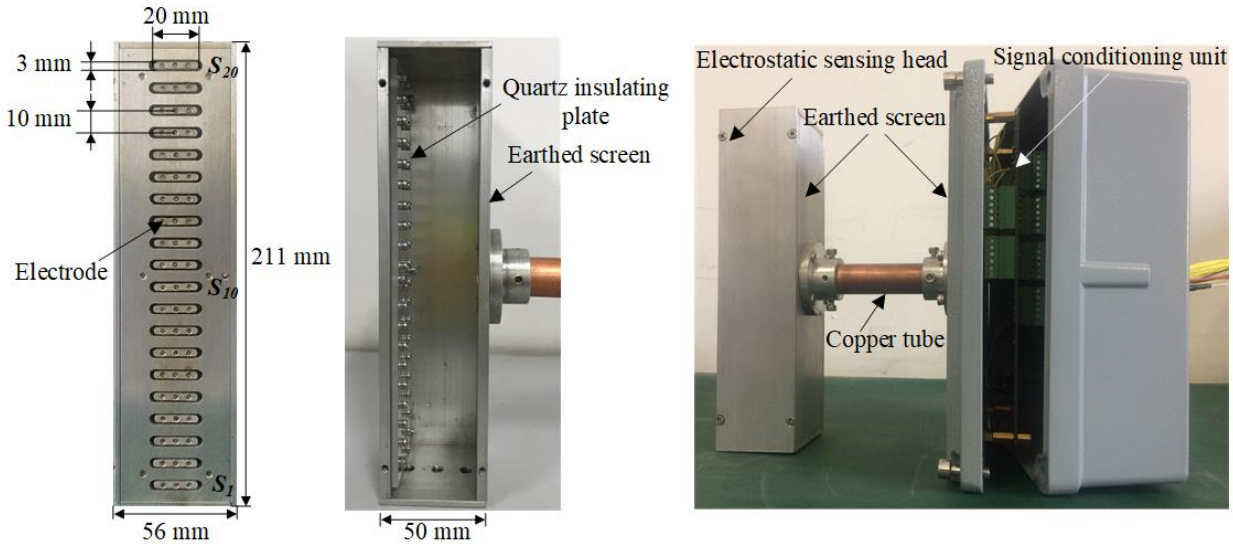

Fig. 2. Design and construction of the electrostatic sensing system. (a) Front view of the sensing head. (b) Side view of the sensing head. (c) Structure of the sensing head.

Comparative studies with isolated electrodes were firstly conducted to investigate the origin of the sensor signal. The difference between an isolated electrode and an exposed electrode is that the former has a quartz insulating strip between the surface of the electrode and the flame. For the isolated electrode, the ions, electrons and charged soot particles in the flame cannot contact with the electrode. Thus the measured signals are completely due to electrostatic induction from the charged species [25]. By contrast, the signals from the exposed electrode are composed of both induced and transferred charge signals [25]. It is worth noting that the sensing electrodes are prone to be contaminated, in particular, by particles and dust in the combustion field. Such contaminants

on electrodes in some applications may affect the sensing process [26]. However, in the vast majority of combustion chambers, dust and soot particles are unlikely to deposit on the electrode surface because of the combustion air continuously flushing over the electrode. The potential contamination of the electrodes by particles has, therefore, little impact on the sensing process in this case.

Fig. 3 illustrates the main stages in the signal conditioning unit. A key element in the signal conditioning unit, the I/V converter as shown in Fig. 4, converts the weak current signal from the electrode into a voltage signal. The electrode is connected to the virtual ground of the operational amplifier, allowing the current to flow through the feedback resistor R_f to generate a voltage output. The feedback resistor R_f in the I/V converter determines the transimpedance gain, while the feedback capacitor C_f ensures stability through phase compensation [27]. The voltage signal is then amplified by a secondary amplifier before being fed into a second-order low-pass filter. Since preliminary experimental results [28] have shown that the main components of the sensor signal in this study are within 30 Hz, the filter is set to have a cut-off frequency of 50 Hz to eliminate high-frequency noise and inhibit signal aliasing.

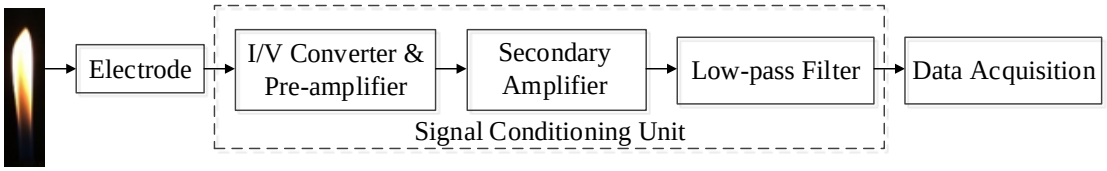

Fig. 3. Main stages in the signal conditioning unit.

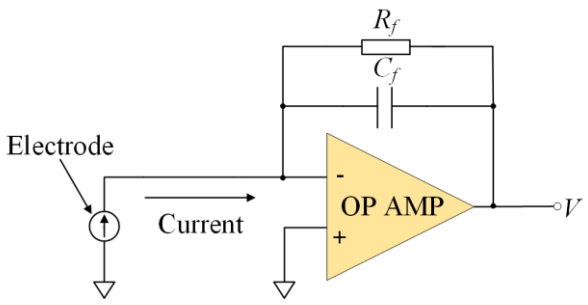

Fig. 4. I/V converter in the signal conditioning unit.

The signal conditioning unit, consisting of 20 parallel sensing channels, was fabricated on a double-side printed circuit board. The circuit board, as shown in Fig. 5, is powered from a ±2.5 V dual supply and connected to the electrodes using independently shielded cables. The signal conditioning unit is enclosed within an earthed screen to avoid external electronic interference. A data acquisition (DAQ) unit samples the 20 signals with a frequency of 250 Hz per channel.

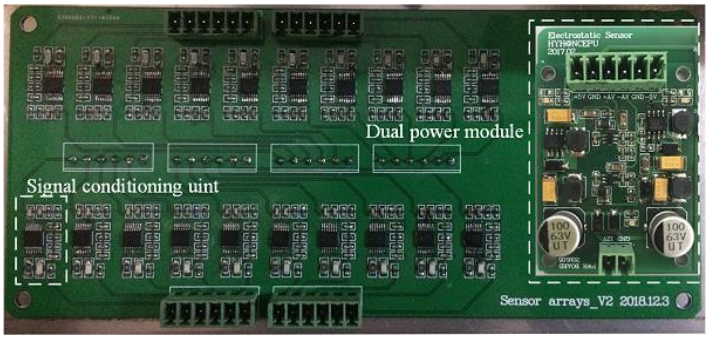

Fig. 5. Signal conditioning circuit board.

III. EXPERIMENTAL RESULTS AND DISCUSSION

A. Experimental Setup

In order to assess the performance of the measurement system, a series of experiments were conducted on a laboratory-scale combustion test rig. As shown in Fig. 6(a), the test rig consists of an air compressor, a high-pressure methane gas holder, a flow rate controller, a burner and a chamber. The flow rates of the air and the methane are metered, controlled and displayed using the flow rate controller during the experiments. Two types of flame can be created by varying the air and fuel flow rates. A diffusion flame is created by varying the fuel flow rate with air supplied from the ambient. Each combustion condition of the premixed flame is identified by the equivalence ratio Φ,

which is recognized as one of the most important factors in relation to fuel conversion, pollutant emissions, heat loss and flame stability [9]. The equivalence ratio, Φ, is defined as:

$$\Phi = \frac{(\text{fuel-to-air ratio})_{\text{actual}}}{(\text{fuel-to-air ratio})_{\text{stoichiometric}}} \tag{4}$$

where the stoichiometric ratio is the chemically correct fuel to air ratio necessary to achieve complete combustion of the fuel. For methane, the stoichiometric ratio is 1:9.52 by volume. To create a premixed flame of a given equivalence ratio Φ, the air flow rate is varied whilst the fuel flow rate is held constant. Either flame is ignited at the burner nozzle in the 80 × 80 × 70 cm^3 chamber which provides a quiescent environment. The diameter of the burner is 24 mm. A mesh screen is mounted across the outlet of the burner to stabilize the flame. The electrostatic sensor array is fixed on a supporting bracket in the proximity of the flame, as shown in Fig. 6(b). Since the maximum flame height under all test conditions is 155 mm, the electrostatic sensor array with an overall height of 211 mm is capable of covering the whole flame. The instantaneous flame shape and its fluctuations can thus be detected using the sensor array. In this study the spacing from the sensor to the center of the burner is set to 25 mm by taking the maximum distance between the electrode and the flame into consideration. A closer spacing between the sensor and the flame helps improve the signal-to-noise ratio, but this is achieved at the expense of an increasing likelihood of direct contact between them which leads to signal saturation. In this study the sensor signals were acquired using a NI USB-6363 DAQ and processed on a host computer.

A digital CMOS RGB color camera (Photron, FASTCAM Mini UX50) was used to acquired flame images, from which the reference distance between the electrode and the flame boundary was determined. Flame images with a resolution of 1280 (H) × 1024 (V) were recorded at a rate of 250 frames per second to keep consistent with the sampling frequency of the signals from the

electrostatic sensor array. The image acquisition of the camera was triggered by a digital output signal from the DAQ to realize the synchronous acquisition of the sensor signals and the flame images. The installation of the electrostatic sensor array and the digital camera on the combustion test rig is illustrated in Fig. 6(a).

The measurement procedure of the reference distance between the electrode and the flame boundary is as follows. Firstly, the flame images captured by the camera are segmented using the Otsu's method [29]. Secondly, the pixel coordinates of the right boundary of the sensor and the left boundary of the flame in the image are extracted respectively. Each pixel point of the boundary is detected by determining the difference of the grey-levels between two adjacent pixels and comparing this with a constant which is equal to 1 for the detection of the left flame boundary and -1 for the detection of the right sensor boundary. Then the distance between the sensor and the flame in pixels at each row is determined by calculating the difference in pixel coordinates between the left boundary of the flame and the right boundary of the sensor. Finally, the distance in pixels is converted into a distance in millimeters with a conversion factor. To obtain the absolute measurement of the distance, the camera has to be calibrated in advance for a given installation. This was achieved by comparing the true distance between the right boundary of the sensor and the left boundary of the burner and the distance obtained using the imaging system. The calculation procedure of the distance from the imaging system is the same as the above reference distance between the electrode and the flame boundary. The accuracy of the method was assessed by measuring a series of distances from 4 mm to 30 mm with an increment of 3 mm. Fig. 7 shows a direct comparison between the measured and true distances. The maximum relative error is found no greater than 3% for all the distances.

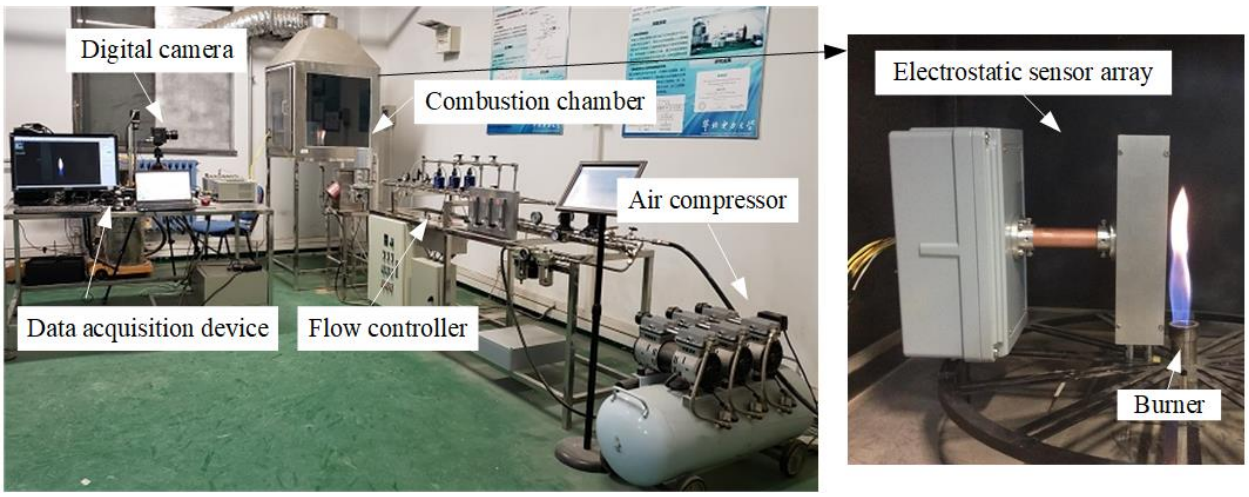

(a) (b)

Fig. 6. Experimental setup. (a) Combustion test rig. (b) Installation of the electrostatic sensor array.

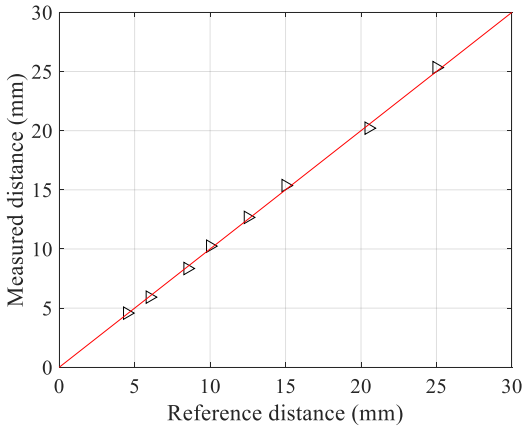

Fig. 7. Comparison between the measured and reference distances.

B. Validation of the Proposed Technique

1) Unipolar Sensor Signals of a Premixed Flame

Fig. 8 shows the typical raw signals from both isolated and exposed electrodes at the equivalence ratio of 1. It is evident that the induced signal from the isolated electrode is bipolar, while the signal due to induced and transferred charges from the exposed electrode is unipolar. The average voltage of the induced signal is almost zero, whereas that of the induced and transferred signal is 55.7 mV. Moreover, the amplitude of the induced signal is negligible in comparison with the signal due to

induced and transferred charges. This is due to the fact that the flame is a weak plasma and electroneutral as a whole. It can be drawn from the results that the signal from the exposed electrode arises primarily from transferred charge. The transferred charge on the electrode arises from a combination of ions, electrons and charged soot particles in contact with the electrode surface. In view of the negligible amplitude of induced charge signal from the isolated electrode, the exposed electrode is used in the following study. Moreover, it is worth noting that the overall polarity of ions, electrons and charged soot particles can be determined from the polarity of the signal from the exposed electrode.

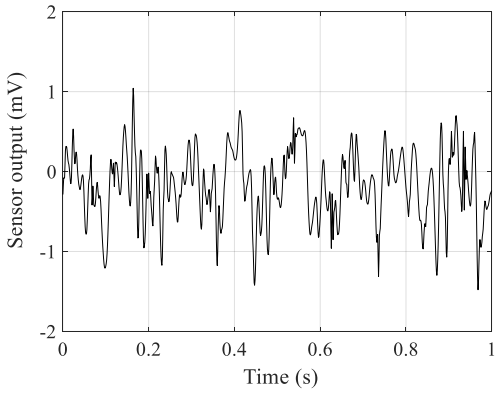

(a)

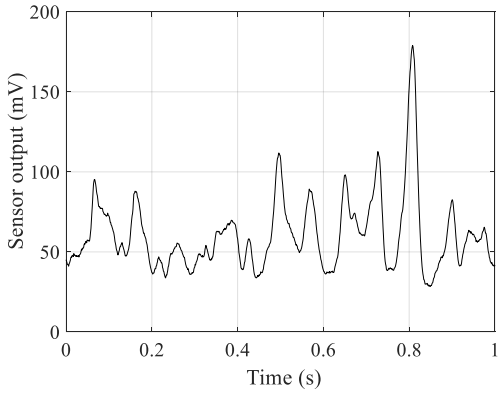

(b)

Fig. 8. Sensor signals at the equivalence ratio of 1. (a) Isolated electrode. (b) Exposed electrode.

2) Effect of the Distance on the Sensor Signal

In order to verify the feasibility of electrostatic sensors for flame boundary measurement, the electrostatic signal and the simultaneous variation of the distance between the electrode and the flame boundary are compared. Fig. 9 shows the signal from sensor S_{11}, as shown in Fig. 2, and the distance measured using the camera when the fuel flow rate for a diffusion flame is 0.6 L/min. Both signals show clear periodicity and similar patterns with inverse phase, suggesting that the two signals are strongly negatively correlated. It can be inferred that the spatial charge density which determines the amount of transferred charge on the electrode increases inversely with the distance between the electrode and the flame boundary. The corresponding power spectral density (PSD) of the sensor signal and the distance in Fig. 9 are plotted in Fig. 10, in which normalization is also performed separately with respect to the highest PSD peak. It is shown that there exist strong PSD peaks in both measurements. With reference to the digital camera, the electrostatic sensor can identify the flame oscillation frequencies accurately. The relative magnitudes of the PSD peaks in both measurements are in good agreement, with slight difference especially for the last two harmonics due to the different sensing mechanisms.

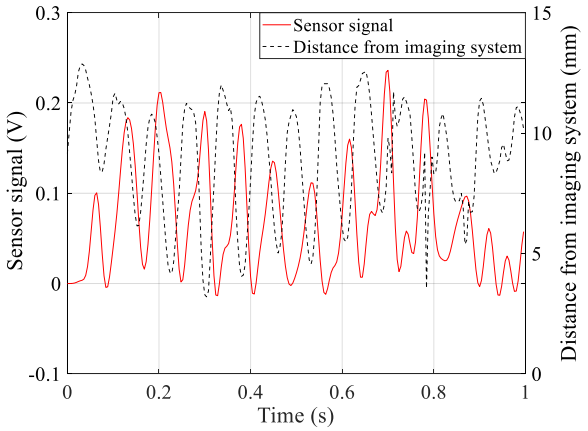

Fig. 9. Signal from the electrostatic sensor and the distance measured from the imaging system for a diffusion flame at a fuel flow rate of 0.6 L/min.

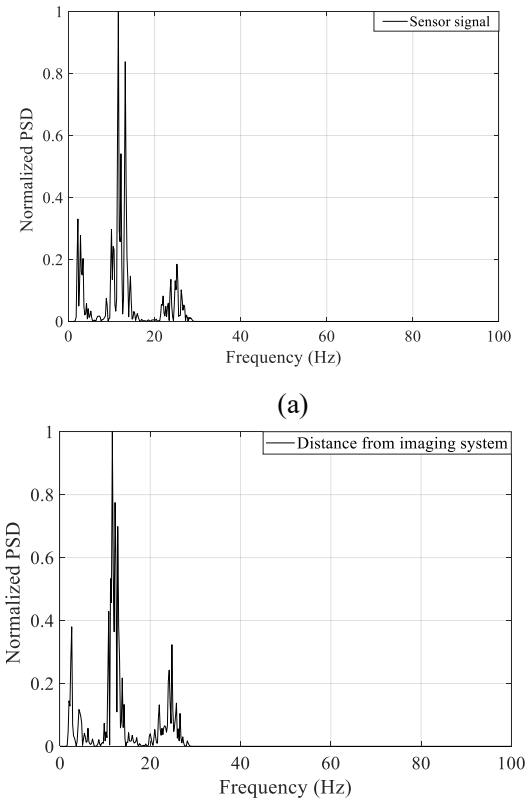

Fig. 10. Normalized PSD of the measurements in Fig. 9. (a) Signal from the electrostatic sensor. (b) Distance measured from the imaging system.

Fig. 11 depicts five typical signals from sensors S_7, S_9, S_{11}, S_{13} and S_{15} at a fuel flow rate of 0.6 L/min for a diffusion flame. Sensors S_7 and S_9, which are located in the region of flame root, generate signals of a smaller fluctuation amplitude because of the increasing distance and weaker fluctuation. Sensors S_{11} and S_{13}, which are located in the middle region of the flame, generate signals of a higher amplitude due to the closer distance between the electrode and the flame. Sensor S_{15} corresponds to the region of the flame tip. The signals from sensors S_{11}, S_{13} and S_{15} exhibit clear periodicity. It is evident that a shorter distance between the flame and the electrode results in a larger amount of transferred charge on the electrode and hence a higher amplitude of the sensor signal. These results imply that the electrostatic sensor can be used for non-contact distance measurement in a combustion environment.

The corresponding PSD of the signals in Fig. 11, but with a duration of 20 s, are plotted in Fig. 12, illustrating that the flame oscillation frequencies are similar along the flame longitudinal direction. Moreover, the diffusion flame appears to have a single dominant frequency and oscillates within a relatively lower frequency range. Such a result is consistent with the observations in previous research using digital imaging techniques [30].

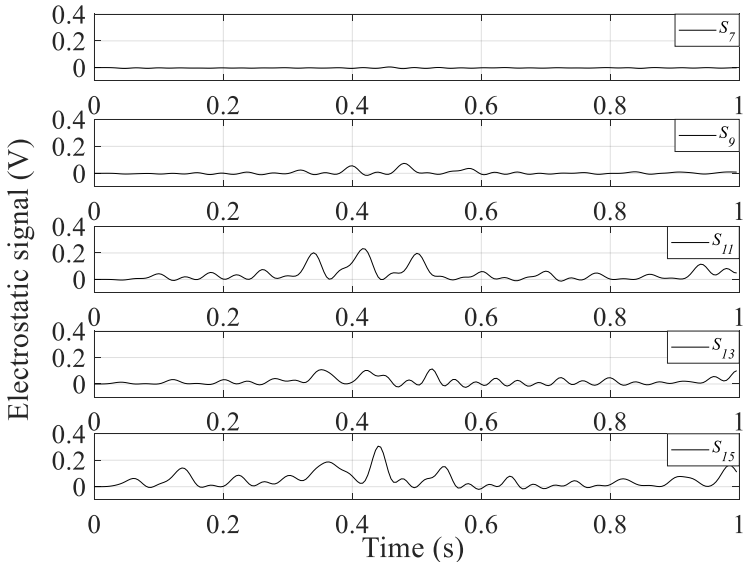

Fig. 11. Typical signals from sensors S_7, S_9, S_{11}, S_{13} and S_{15} for a diffusion flame at a fuel rate of 0.6 L/min.

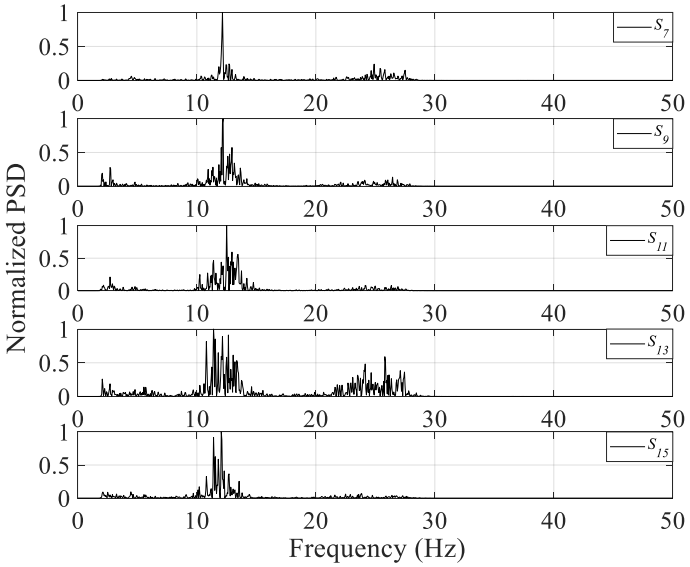

Fig. 12. Normalized PSD of the sensor signals in Fig. 11.

C. Measurement Results of Flame Boundary

1) Determining the Distance Between the Electrode and the Flame Boundary

In order to determine the absolute distance between the electrode and the flame boundary under different operating conditions, regression analysis of the average magnitude of the sensor signal and the corresponding average distance is performed to determine the relationship between the sensor signal and the distance. For a premixed flame at $\Phi = 1.52$, the flame tip can reach up to the 10^{th} electrode. Each sensor signal with a total duration of 5 s is divided into ten data segments, and then the average magnitude of each data segment is determined. The average of the ten individual magnitude values for each sensor corresponds to the abscissa of each data point in Fig. 13. Similarly, ten average measurements of the distance between each sensor and the flame are acquired from the imaging system. The average of the ten distance measurements for each sensor corresponds to the ordinate of each data point in Fig. 13. The standard deviation of each data point in Fig. 13 is given as error bars. It can be observed that the average magnitude of the sensor signal decreases with the distance between the electrode and the flame. The standard deviations of data points at smaller distances are larger as a consequence of a more significant fluctuation of the flame tip in the axial direction. The measured data points can be fitted to a curve through exponential curve fitting method, which has the best performance in this study in comparison with power and polynomial fitting methods. The fitted curve is governed by the following equation that describes the relationship between the sensor signal and the distance

$$d = a_0 e^{-a_1 U} + b_0 e^{-b_1 U} \qquad (5)$$

where U is the average magnitude of the signal from the electrostatic sensor and a_0, a_1, b_0 and b_1 are coefficients that mainly relate to fuel properties and burner type. Note that the coefficients need

to be determined through experimental calibration for different fuels, burners and combustion processes. The specific form of equation (5) derived from the fitted curve in Fig. 13 is as follows

$$d = 11.59e^{-242.70U} + 11.16e^{-2.84U} \quad (6)$$

Equation (6) indicated the fitted curve in Fig. 13 is a combination of two independent exponential functions. The first term in equation (6) represents dominantly the long distance whereas the second term the shorter distance. When the magnitude is measured from the sensor signal, the distance between the electrode and the flame can be determined by solving equation (6) numerically. The flame boundary is finally reconstructed from a set of distance measurements.

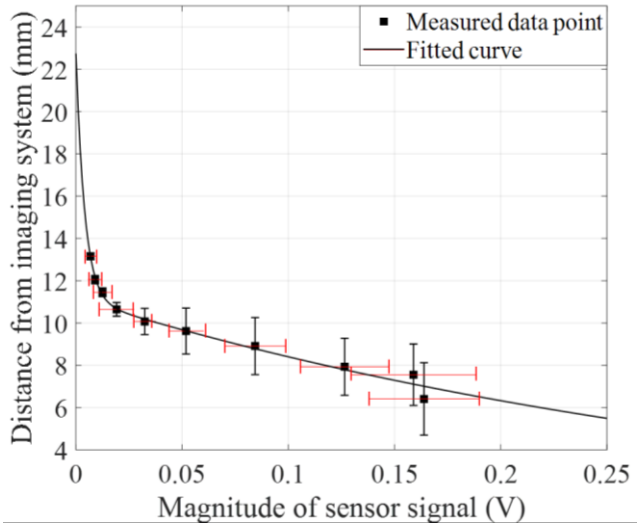

Fig. 13. Regression curve between the sensor signal and the distance from the imaging system.

2) Measurement Results Using Instantaneous Sensor Signals

Fig. 14 shows the reconstructed left boundaries of the flame using the instantaneous sensor signals with regression equation (6) and the reference boundaries obtained from flame images for two types of flame: (a) a diffusion flame at the fuel flow rate of 0.7 L/min and (b) a premixed flame at the equivalence ratio of 3.81. As can be seen, the first column shows the instantaneous flame image, the second column shows the reconstructed left boundary using the amplitude magnitude of the instantaneous sensor signal and the reference left boundary from the imaging system. It is evident

that the reconstructed and reference flame boundaries have similar profiles, but the absolute distances are different, especially for the flame root and tip regions. In the flame root region, the distance measurements are smaller than the reference distances. It is because that the weak fluctuation of flame root region and smaller amplitude of the sensor signal due to the increased distance bring about larger measurement errors. The distance measurements in the flame tip region are larger than the reference distances, which is in accordance with the situation that at smaller distances the measured data points in Fig. 13 deviate largely from the fitted curve.

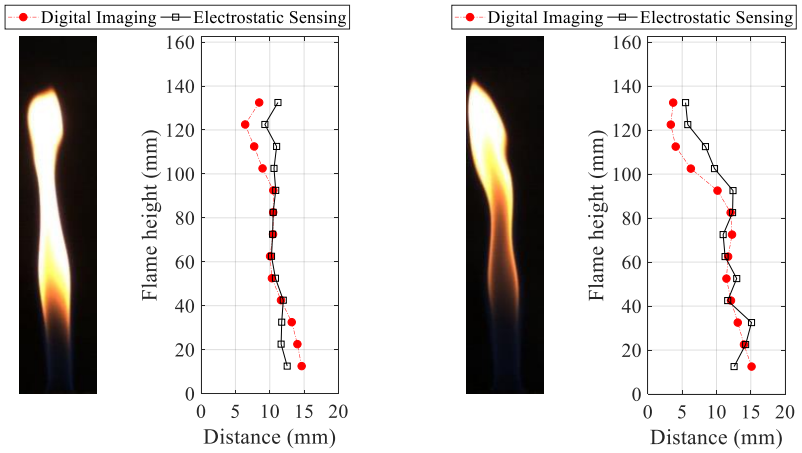

Fig. 14. Reconstructed left boundaries of the flame with reference values from the imaging system. (a) Diffusion flame at the fuel flow rate of 0.7 L/min. (b) Premixed flame at the equivalence ratio of 3.81.

3) Measurement Results Using the Average Magnitude of Sensor Signal

In order to optimize the measurement results, the average magnitude of the sensor signal is used to reconstruct the flame boundary. Five test conditions of diffusion flames were created by varying the fuel flow rate over the range of 0.60-0.80 L/min with an increment of 0.05 L/min. Average diffusion flame images of 1250 instantaneous images taken under each test condition are shown in Fig. 15. It is evident that the flame height increases with the fuel flow rate. The reason for this is that the luminous soot particles in the fuel-lean region of the flame extend the flame height as the

fuel flow rate increases. For a higher fuel flow rate, the flame is more luminous due to the phenomenon that the yellow (soot-containing) region becomes wider. Fig. 16 illustrates the reconstructed left boundaries using the average magnitude of the sensor signal with reference to the left boundaries obtained from flame images under the five test conditions. It is obvious that the reconstructed outcomes are in good agreement with the reference results for all five flames, although the measured distances are slightly larger than the reference values.

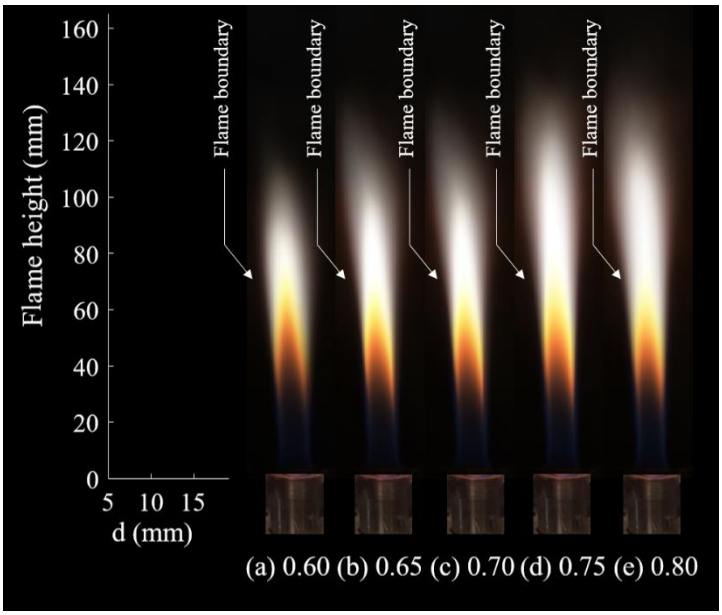

Fig. 15. Average diffusion flame images at five fuel flow rates.

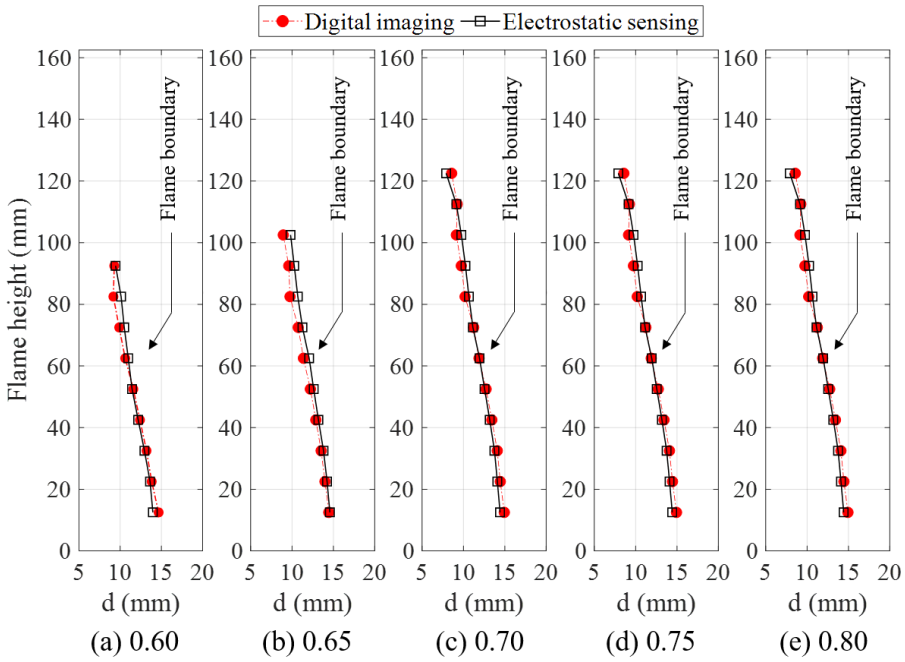

Fig. 16. Reconstructed left boundaries of the flame with reference values from the imaging system under the test conditions considered in Fig. 15.

Five test conditions of premixed flames (Φ=1.27-3.81) were created by varying the air flow rate over the range of 2-6 L/min with an increment of 1 L/min at a fixed fuel flow rate of 0.8 L/min. Average premixed flame images of 1250 instantaneous images taken at each equivalence ratio are shown in Fig. 17. It can be seen that the height of the premixed flame increases with the equivalence ratio. This is due to the fact that the luminous soot particles in the fuel-lean region of the flame result in an elongated flame for a higher equivalence ratio. The flame brightness increases with the equivalence ratio, too, which is attributed to the phenomenon that the yellow (soot-containing) region becomes wider and the blue (soot- free) region narrower. Fig. 18 illustrates the reconstructed left boundaries using the average magnitude of the sensor signal with reference to the left boundaries obtained from flame images under the five test conditions. In comparison with the measurement results of diffusion flames, the measured distances in the root region of premixed flames are larger than the reference values. An explanation for this is that, in the bigger area of the

blue region for the premixed flame, the sensor signal exhibits a smaller fluctuation amplitude due to the increasing distance and weaker fluctuation, which leads to larger errors in the measured distances.

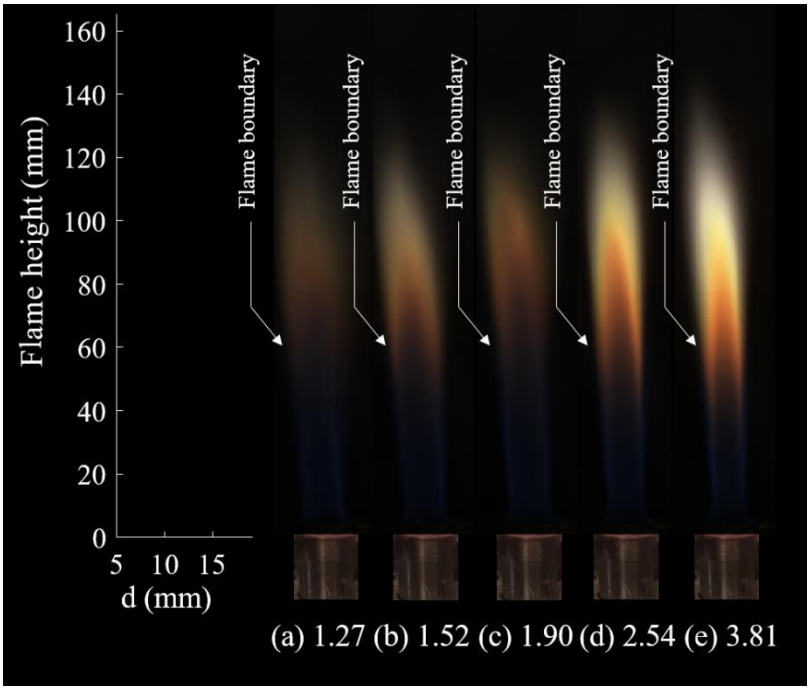

Fig. 17. Average premixed flame images at five equivalence ratios.

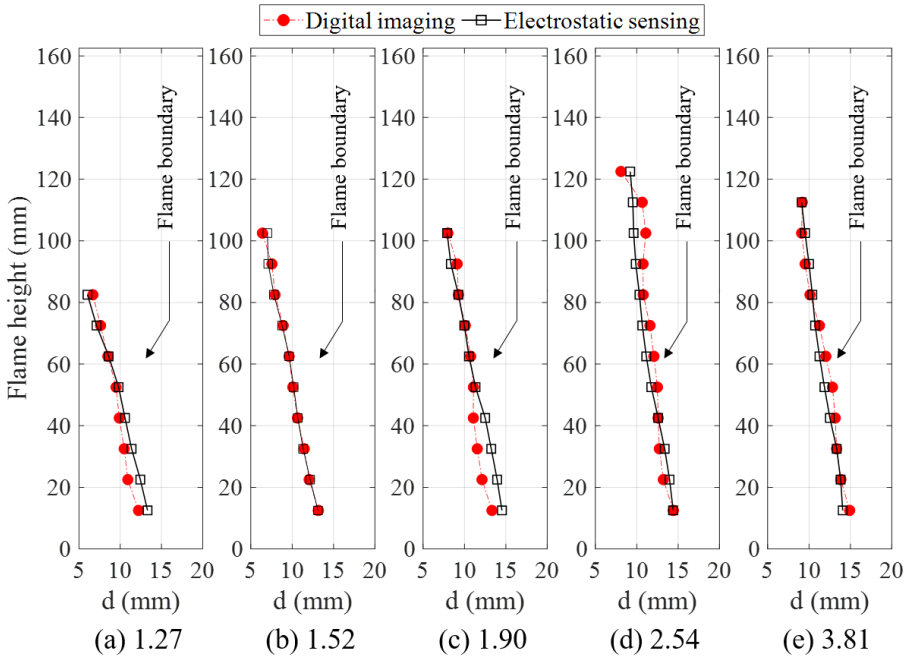

Fig. 18. Reconstructed left boundaries of the flame with reference values from the imaging system under the test conditions considered in Fig. 17.

D. Evaluation of the Reconstructed Flame Boundary

To evaluate the reconstructed flame boundary, correlation coefficient, mean relative error and relative root mean square error are computed to compare the measured and reference results, which have been widely used as valid indexes for quality evaluation of reconstructed results. The correlation coefficient between the reconstructed and reference flame boundaries *CC*, the mean relative error *MRE* and the relative root mean square error *RRMSE* of the reconstructed flame boundary can be calculated respectively from

$$CC = \frac{\sum_{i=1}^{N}(D_i - \overline{D})(d_i - \overline{d})}{\sqrt{\sum_{i=1}^{N}(D_i - \overline{D})^2 \sum_{i=1}^{N}(d_i - \overline{d})^2}} \tag{7}$$

$$RRMSE = \left(\frac{\sum_{i=1}^{N}(d_i - D_i)^2}{\sum_{i=1}^{N} D_i^2} \right)^{0.5} \tag{8}$$

$$MRE = \frac{1}{N}\sum_{i=1}^{N}\left(\frac{|d_i - D_i|}{D_i} \times 100\%\right) \tag{9}$$

where D_i is the i^{th} reference distance measured using the camera, d_i is the distance measured using the i^{th} electrostatic sensor, and N is the number of electrostatic sensors covering the whole flame under the test conditions. $\overline{D}$ and $\overline{d}$ denote the mean values of D_i and d_i, respectively.

The results of the reconstructed flame boundary in Fig. 17 and Fig. 18 are summarized in Table I. It can be seen that the *CC* of diffusion flames under all test conditions are larger than 0.98, the *MRE* within 4.8% and the *RRMSE* less than 0.05. For premixed flames, the *CC* for all test conditions are mostly larger than 0.96, the *MRE* within 7.4% and the *RRMSE* mostly less than 0.09. The

reconstructed outcomes for the diffusion flames show a better agreement with the reference results than those for the premixed flames.

Table I. Evaluation results for the reconstructed flame boundaries in Fig. 17 and Fig. 18.

Flame type	Fuel flow rate (L/min)	Φ	*CC*	*MRE*	*RRMSE*
Diffusion flame	0.60	/	0.989	3.65%	0.0409
	0.65		0.998	4.80%	0.0482
	0.70		0.995	1.57%	0.0173
	0.75		0.987	2.7%	0.0282
	0.80		0.985	3.18%	0.0337
Premixed flame	/	3.81	0.974	3.87%	0.0467
		2.54	0.891	6.87%	0.0729
		1.90	0.964	6.66%	0.0950
		1.52	0.992	2.25%	0.0254
		1.27	0.994	7.38%	0.0866

IV. CONCULSIONS

A novel instrumentation system using an electrostatic sensor array has been designed and implemented to measure the boundary of a burner flame. The signal from the exposed electrode has been found to be unipolar, which arises primarily from transferred charge because the flame is electroneutral as a whole. The feasibility of the proposed technique has been verified on a laboratory-scale combustion test rig in comparison with the established digital imaging method. Results obtained have demonstrated that the signal from the electrostatic sensor and the distance variation of the diffusion flame have clear periodicity and similar patterns with inverse phase, which permits the measurement of distance using the electrostatic signal. Exponential regression analysis has been conducted to establish the relationship between the sensor signal and the distance variation. The boundaries for diffusion and premixed flames have been reconstructed using a set of distance measurements obtained from the electrostatic sensor array.

Correlation coefficient between the reconstructed and reference flame boundaries and mean square error and relative root mean square error of the reconstructed flame boundary have been adopted to evaluate the measurement results. For diffusion flames over the range of air flow rates 2-6 L/min and premixed flames over the range of equivalence ratios 1.27-3.81, the measurement system performs well with a correlation coefficient mostly larger than 0.96, mean relative error within 7.4% and relative root mean square error within 0.09. The results have suggested that better measurement outcomes are achieved for the diffusion flames than the premixed flames. The reason for this is that, in the bigger area of the blue region for the premixed flame, the sensor signal exhibits a smaller fluctuation amplitude due to the increased distance and weaker fluctuation, resulting in larger errors in the measured distances. Moreover, the overall polarities of ions, electrons and charged soot particles in the diffusion and premixed flames can be determined from the polarities of sensor signals.

Future work will focus on the performance assessment of the measurement system for different fuels and burners under a wider range of conditions. Two-dimensional reconstruction and three-dimensional visualization of the flame shape will also be attempted.

ACKNOWLEDGMENT

The authors wish to acknowledge the National Natural Science Foundation of China (No. 61673170 and No. 51827808), the Fundamental Research Funds for the Central Universities (No.2019QN043) for providing financial support for this research. The IEEE Instrumentation and Measurement Society is acknowledged for offering an IEEE Graduate Fellowship Award in relation to the research reported in this paper.

References

[1] M. A. Attar, H. Zhao, M. R. Herfatmanesh and A. Cairns, "Turbulent flame boundary and structure detection in an optical DISI engine using tracer-based two-line PLIF technique," *Exp. Therm. Fluid. Sci.*, vol. 68, pp. 545–558, 2015.

[2] S. S. Krishnan, J. M. Abshire, P. B. Sunderland, Z. G. Yuan and J. P. Gore, "Analytical predictions of shapes of laminar diffusion flames in microgravity and earth gravity," *Combust. Theor. Model.*, vol. 12, no. 4, pp. 605–620, 2008.

[3]J. Fang, J. Wang, J. Guan, Y. Zhang and J. Wang, "Momentum- and buoyancy-driven laminar methane diffusion flame shapes and radiation characteristics at sub-atmospheric pressures," Fuel, vol. 163, no. 1, pp. 295–303, 2016.

[4]P. B. Sunderland, J. G. Quintiere, G. A. Tabaka, D. Lian and C. W. Chiu, "Analysis and measurement of candle flame shapes," *Proc. Combust. Inst.*, vol. 33, no. 2, pp. 2489–2496, 2011.

[5]S. Lee, S. Seo, J. C. Broda, S. Pal and R. J. Santoro, "An experimental estimation of mean reaction rate and flame structure during combustion instability in a lean premixed gas turbine combustor," *Proc. Combust. Inst.*, vol. 28, no. 1, pp. 775–782, 2000.

[6]F. Parsinejad, M. Matlo and M. Metghalchi, "A mathematical model for schlieren and shadowgraph images of transient expanding spherical thin flames," *J. Eng. Gas Turb. Power*, vol. 126, no. 2, pp. 241–247, 2004.

[7]F. Parsinejad, J. C. Keck, and H. Metghalchi, "On the location of flame edge in shadowgraph pictures of spherical flames: a theoretical and experimental study," *Exp. Fluids*, vol. 43, pp. 887–894, 2007.

[8]Y. Hardalupas, A. Selbach and J. H. Whitelaw, “Aspects of oscillating flames,” *J. Visual.*, vol. 1, no. 1, pp. 79–85, 1998.

[9]D. Sun, G. Lu, H. Zhou and Y. Yan, “Condition monitoring of combustion processes through flame imaging,” *Combust. Sci. Technol.*, vol. 185, no. 9, pp. 1400–1413, 2013.

[10] T. Qiu, Y. Yan and G. Lu, “An autoadaptive edge-detection algorithm for flame and fire image processing,” *IEEE Trans. Instrum. Meas.*, vol. 61, no. 5, pp. 1486–1493, 2012.

[11] Z. Wei and J. Qiao, “Industrial flame edge detection algorithm based on gray dominant filter,” *Int. J. Multimed. Ubiquit. Eng.*, vol. 10, no. 2, pp. 87–96, 2015.

[12] J. Lawton and F. J. Weinburg. Electrical Aspects of Combustion. Oxford, U.K: Clarendon Press, 1969.

[13] J. Guo, J. M. Goodings, A. N. Hayhurst and S. G. Taylor, “A simple method for measuring positive ion concentrations in flames and the calibration of a nebulizer/atomizer,” *Combust. Flame.*, vol. 133, pp. 335–343, 2003.

[14] T. Addabbo, A. Fort, M. Mugnaini, L. Parri, V. Vignoli, M. Allegorico, M. Ruggiero and S. Cioncolini, “Ion sensor-based measurement systems: application to combustion monitoring in gas turbines,” *IEEE Trans. Instrum. Meas.*, vol. 69, no. 4, pp. 1474–1483, 2020.

[15] R. C. Waterfall, R. He and C. M. Beck, “Visualizing combustion using electrical impedance tomography,” *Chem. Eng. Sci.*, vol. 52, no. 13, pp. 2129–2138, 1997.

[16] W. Zhang, Y. Yan, Y. Yang and J. Wang, “Measurement of flow characteristics in a bubbling fluidized bed using electrostatic sensor arrays,” *IEEE Trans. Instrum. Meas.*, vol. 65, no. 3, pp. 703–712, 2016.

[17] J. R. Coombes and Y. Yan, "Measurement of velocity and concentration profiles of pneumatically conveyed particles using an electrostatic sensor array," *IEEE Trans. Instrum. Meas.*, vol. 65, no. 5, pp. 1139–1148, 2015.

[18] L. Wang, Y. Yan, Y. Hu and X. Qian, "Rotational speed measurement through electrostatic sensing and correlation signal processing," *IEEE Trans. Instrum. Meas.*, vol. 63, no. 5, pp. 1190–1199, 2014.

[19] Y. Hu, Y. Yan, L. W, X. Qian and X. Wang, "Simultaneous measurement of belt speed and vibration through electrostatic sensing and data fusion," *IEEE Trans. Instrum. Meas.*, vol. 65, no. 5, pp. 1130–1138, 2016.

[20] L. B. W. Peerlings, Manohar, V. N. Kornilov and P. D. Goey, "Flame ion generation rate as a measure of the flame thermo-acoustic response," *Combust. Flame*, vol. 160, no. 11, pp. 2490–2496, 2013.

[21] K. Schofiel, "The enigmatic mechanism of the flame ionization detector: Its overlooked implications for fossil fuel combustion modeling," *Prog. Energy Combust. Sci.*, vol. 34, no. 3, pp. 330–350, 2008.

[22] M. Balthasa, F. Mauss and H. Wang, "A computational study of the thermal ionization of soot particles and its effect on their growth in laminar premixed flames," *Combust. Flame*, vol. 129, no. 1-2, pp. 204–216, 2002.

[23] H. F. Calcote and D. G. Keil, "The role of ions in soot formation," *Pure Appl. Chem.*, vol. 62, no. 5, pp. 815–824, 1990.

[24] A. B. Fialkov, "Investigations on ions in flames," *Prog. Energy Combust. Sci.*, vol. 23, no. 5-6, pp. 399–528, 1997.

[25] Y. Hu, Y. Yan, X. Qian and W. Zhang, "A comparative study of induced and transferred charges for mass flow rate measurement of pneumatically conveyed particles," *Powder Technol.*, vol. 356, pp. 715–725, 2019.

[26] N. Stan, F. Seng, L. Shumway, R. King and S. Schultz, "Non-perturbing voltage measurement in a coaxial cable with slab-coupled optical sensors," *Appl. optics*., vol. 56, no. 24, pp. 6814–6821, 2017.

[27] S. Franco, Design With Operational Amplifiers and Analog Integrated Circuits, 4th ed. New York, USA: McGraw-Hill, 2014.

[28] J. Wu, Y. Hu, Y. Yan, X. Qian and S. Gu, "Flicker measurement of burner flames through electrostatic sensing and spectral analysis," in *proc. J. Phys.*, *Conf. ser.*, Belfast, U. K., Sep. 2018, Art. no. 202004.

[29] X. Bai, G. Lu, T. Bennet, A. Sarroza, C. Eastwick, H. Liu and Y. Yan, "Combustion behavior profiling of single pulverized coal particles in a drop tube furnace through high-speed imaging and image analysis," *Exp. Therm. Fluid. Sci.*, vol. 85, pp. 322–330, 2017.

[30] Y. Huang, Y. Yan, G. Lu and A. Reed, "On-line flicker measurement of gaseous flames by image processing and spectral analysis", *Meas. Sci. Technol.*, vol. 10, pp. 726–733, 1999.